Supplement of The Cryosphere, 16, 3867–3887, 2022
https://doi.org/10.5194/tc-16-3867-2022-supplement

The Cryosphere
Open Access

Supplement of

Inverting ice surface elevation and velocity for bed topography and slipperiness beneath Thwaites Glacier

Helen Ockenden et al.

Correspondence to: Helen Ockenden (h.ockenden@sms.ed.ac.uk)

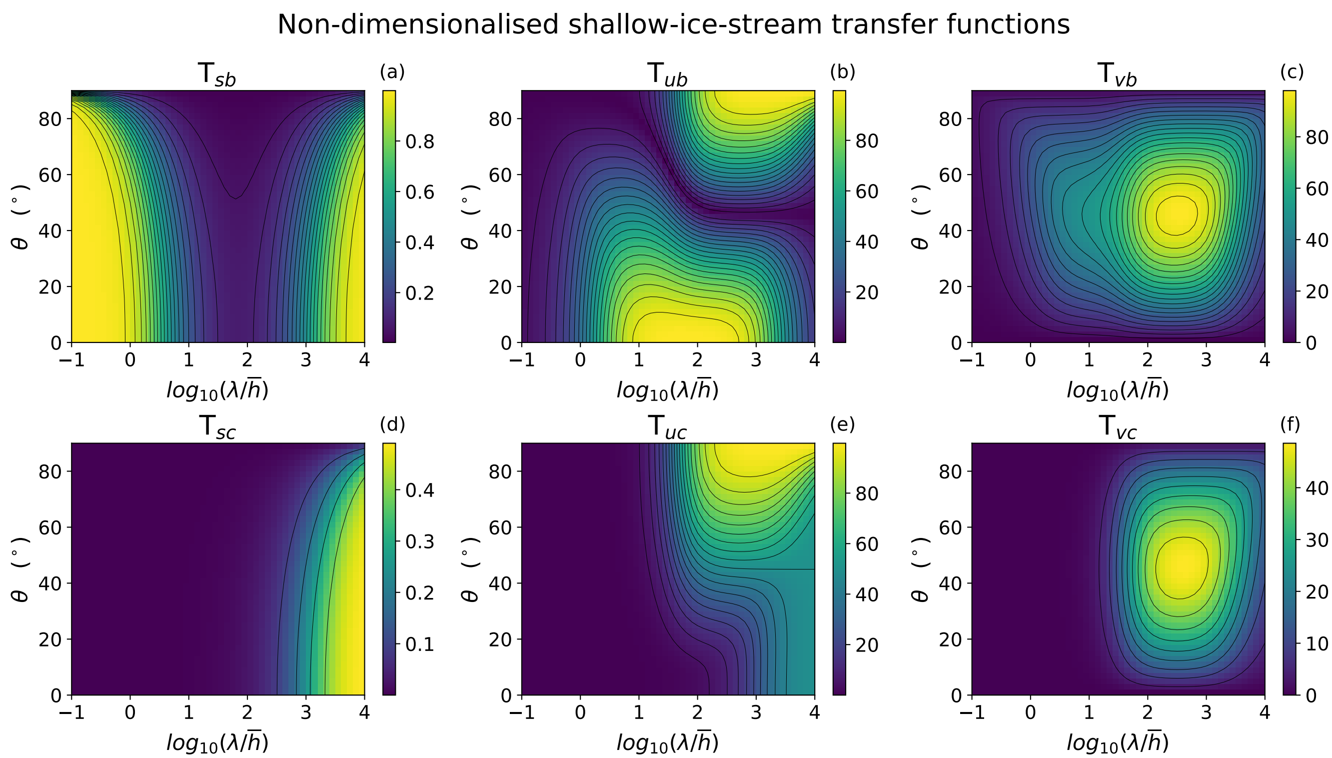

Figure S1. Panels (a), (b) and (c) show the non-dimensional shallow-ice-stream transfer functions T_{SB}, T_{UB} and T_{VB} between non-dimensional bed topography B and surface topography S; along flow velocity U; and across flow velocity V, respectively. Panels (d), (e) and (f) show the non-dimensional shallow-ice-stream transfer functions T_{SC}, T_{UC} and T_{VC} between non-dimensional bed slipperiness C and surface topography S; along flow velocity U; and across flow velocity V, respectively. All transfer functions are calculated for mean slipperiness $\bar{C} = 100$, sliding law constant $m = 1$, and mean surface slope $\alpha = 0.002$. θ is the angle of basal variability to the direction of flow, such that $\theta = 0$ for landforms aligned with the ice flow, and $\theta = 90$ for landforms perpendicular to the ice flow. λ is the wavelength of variability and is non-dimensionalised in terms of $\bar{h}$, the mean ice thickness, such that $\log_{10}(\lambda/\bar{h}) = 1$ means that $\lambda = 10\bar{h}$. $T_{sb} = 0.1$ means that variability in the surface topography will have one tenth of the amplitude of variability in the bed topography at that angle and wavelength. Similar figures can be seen in Gudmundsson (2008) with $\bar{C} = 99$.

S1 Non-dimensionalisation

The form of these transfer functions can be simplified by considering them in a non-dimensional form. For this purpose the same scalings as used in Gudmundsson (2003) and Gudmundsson (2008) are employed.

All spatial scales are in units of mean ice thickness ($\bar{h}$), and stress components in units of driving stress (τ_d).

The non-dimensional form of the equations is obtained using the substitutions $\bar{c} \mapsto \bar{C}$, $\eta \mapsto 1/2$, $\bar{h} \mapsto 1$, $\bar{u} \mapsto \bar{C}$, $k \mapsto k$, $l \mapsto l$, $\gamma \mapsto (m\bar{C})^{-1}$, and $\tau_d = \rho g \bar{h} \sin\alpha \mapsto 1$.

Using these substitution leads to the non-dimensionalised transfer functions, shown in Figure S1:

$$T_{SB}(k,l) = \frac{k\Big(1+m\big(2j^2\bar{C}+1\big)\Big)}{k+m\Big(k+2kj^2\bar{C}+\mathrm{i}j^2\cot\alpha\Big)} \quad \text{(13 non-dimensionalised)}$$

$$T_{UB}(k,l) = \frac{-\mathrm{i}\cot\alpha\Big(l^2m-k^2\big(1+0.5j^2m\bar{C}\big)\Big)}{\Big(k+m\big(k+2kj^2\bar{C}+\mathrm{i}j^2\cot\alpha\big)\Big)\Big((m\bar{C})^{-1}+0.5j^2\Big)} \quad \text{(14 non-dimensionalised)}$$

$$T_{VB}(k,l) = \frac{\mathrm{i}kl\Big(1+0.5j^2mC+m\Big)\cot\alpha}{\Big(k+m\big(k+2kj^2\bar{C}+\mathrm{i}j^2\cot\alpha\big)\Big)\Big((m\bar{C})^{-1}+0.5j^2\Big)} \quad \text{(15 non-dimensionalised)}$$

$$T_{SC}(k,l) = \frac{k}{k+m\Big(k+2kj^2\bar{C}+\mathrm{i}j^2\cot\alpha\Big)} \quad \text{(21 non-dimensionalised)}$$

$$T_{UC}(k,l) = \frac{\bar{C}\Big(3kl^2m\bar{C}+2k+kj^2m\bar{C}+2il^2\cot\alpha m\Big)}{\Big(k+m\big(k+2kj^2\bar{C}+\mathrm{i}j^2\cot\alpha\big)\Big)\Big(2+j^2m\bar{C}\Big)} \quad \text{(22 non-dimensionalised)}$$

$$T_{VC}(k,l) = \frac{-klm\bar{C}\Big(2i\cot\alpha+3k\bar{C}\Big)}{\Big(k+m\big(k+2kj^2\bar{C}+\mathrm{i}j^2\cot\alpha\big)\Big)\Big(2+j^2m\bar{C}\Big)} \quad \text{(23 non-dimensionalised)}$$

S2 Additional airborne radar flight lines

There are 9 airborne radar flight lines from the 2019/2020 field season which cross the region of Thwaites Glacier where the inversion procedure was carried out. 2 of these are presented in the main body of the text, and the remaining 7 are presented here.

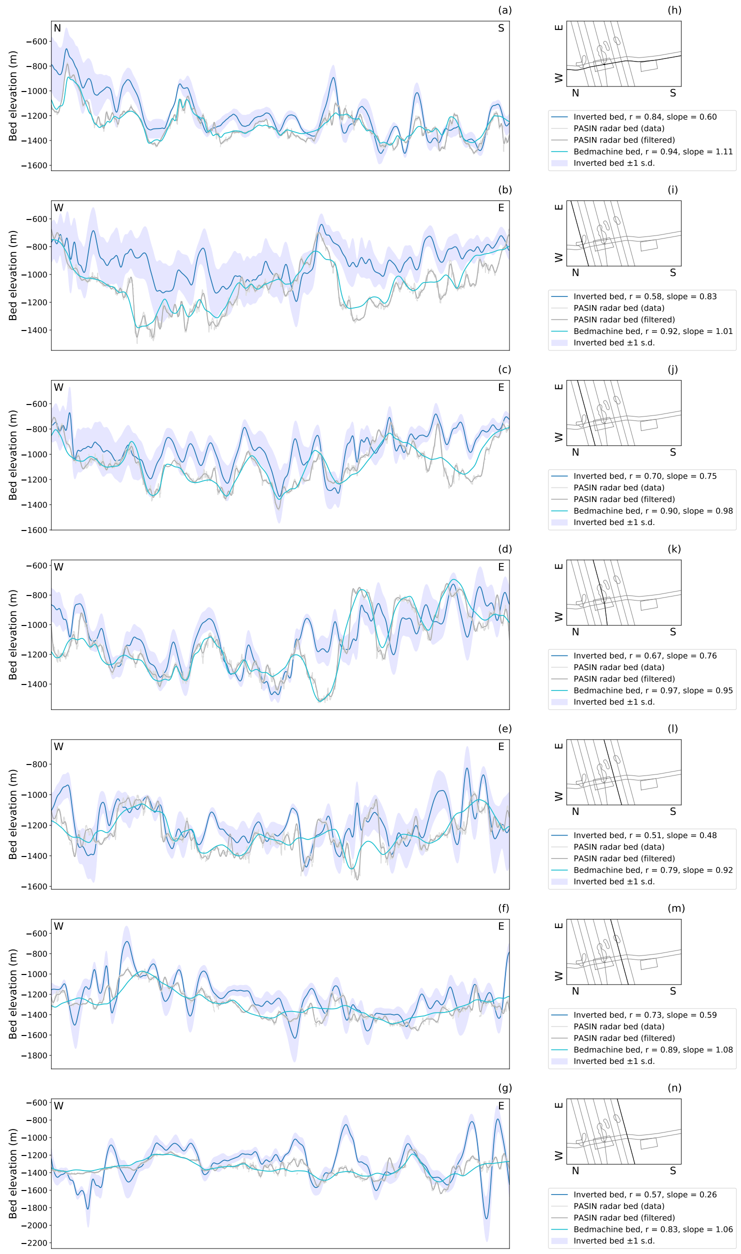

Figure S2. a) to g) Comparative plots of inverted bed topography with mean non-dimensional slipperiness $\bar{C} = 100$ with along flow radar-sounded bed topography. Bed topography is given as unfiltered bed picks from the 2019/20 airborne surveys; a version of he same filtered to 2 km wavelengths to be more representative of the detail we might expect to image in our inversion; and the bed profile extracted from BedMachine Antarctica (Morlighem et al., 2020). The envelope around the inverted bed topography shows plus or minus one standard deviation. The correlation coefficients (r) and slopes given are the results of a linear regression between the inverted bed or the BedMachine Antarctica bed and the filtered radar bed. h) to n) Profile locations within the inverted grid.

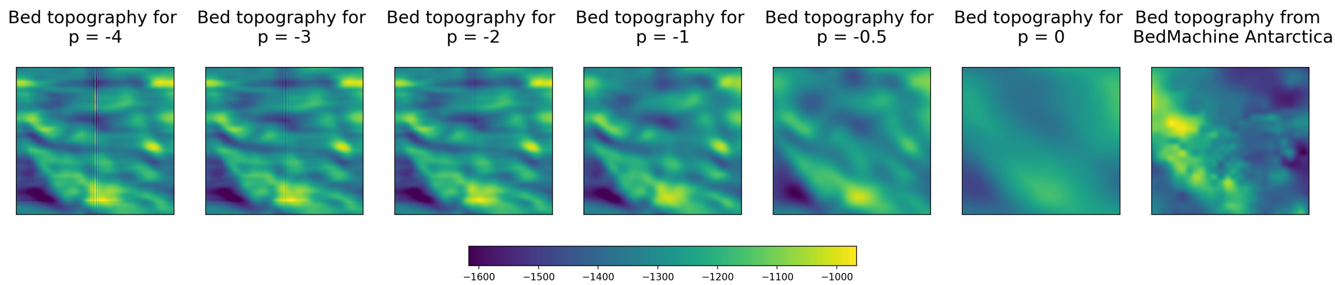

Figure S3. Bed topography results of the inversion for the Upper Thwaites region (see Figure 6 for location) with a variety of values of p_{filt}. Increasing p filters out increasing long wavelengths, and so a value of $p_{filt} = -2$ is chosen to filter out noisy short wavelengths, while maintaining realistic bed features, as compared to Bedmachine Antarctica (Morlighem et al., 2020).

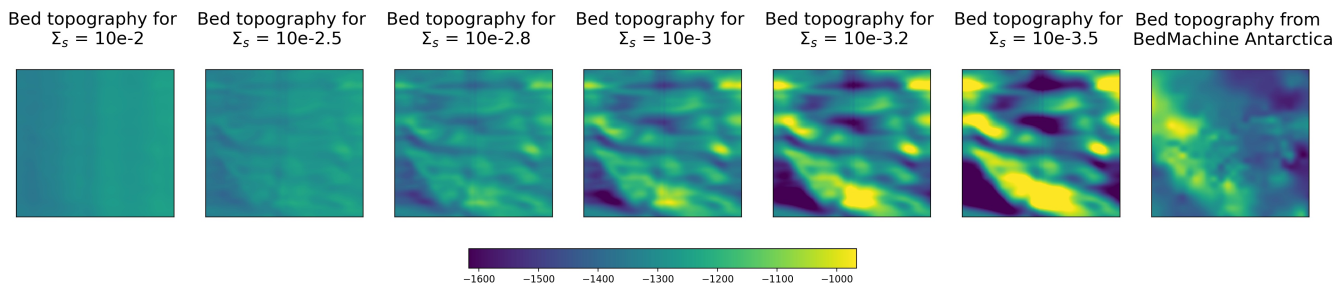

Figure S4. Bed topography results of the inversion for the Upper Thwaites region (see Figure 6 for location) with a variety of values of Σ_s. The weighting factor Σ_s controls the balance in the least squares inversion between the surface elevation and surface velocity data, with smaller values of Σ_s weighting the inversion towards the surface elevation. A value of Σ_s = 0.001 is chosen to produce realistic amplitude bed features, as compared to Bedmachine Antarctica (Morlighem et al., 2020).

S3 Parameter values

The filtering parameter p_{filt} controls which frequencies are suppressed in the inversion to avoid introducing singularities. Higher values of p_{filt} (closer to 0), will filter out higher frequencies (lower wavelengths), and so a value of $p_{filt} = -2$ is chosen to filter out noisy short wavelengths, while maintaining realistic bed features. The weighting factor Σ_s controls the balance in the inversion between the surface elevation and surface velocity data, with smaller values of Σ_s weighting the inversion towards the surface data. Varying p_{filt} and Σ_s for the inversion of the real surface data confirms the choice of values from the synthetic tests ($p_{filt} = -2$, $\Sigma_s = 0.001$) as sensible values which return the best match with real bed data (Figures S3 and S4).

References

Gudmundsson, G. H.: Transmission of basal variability to a glacier surface, Journal of Geophysical Research: Solid Earth, 108, 2253, https://doi.org/10.1029/2002JB002107, 2003.

Gudmundsson, G. H.: Analytical solutions for the surface response to small amplitude perturbations in boundary data in the shallow-ice-stream approximation, The Cryosphere, 2, 77–93, https://doi.org/10.5194/tc-2-77-2008, 2008.

Morlighem, M., Rignot, E., Binder, T., Blankenship, D., Drews, R., Eagles, G., Eisen, O., Ferraccioli, F., Forsberg, R., Fretwell, P., Goel, V., Greenbaum, J. S., Gudmundsson, H., Guo, J., Helm, V., Hofstede, C., Howat, I., Humbert, A., Jokat, W., Karlsson, N. B., Lee, W. S., Matsuoka, K., Millan, R., Mouginot, J., Paden, J., Pattyn, F., Roberts, J., Rosier, S., Ruppel, A., Seroussi, H., Smith, E. C., Steinhage, D., Sun, B., Broeke, M. R. v. d., Ommen, T. D. v., Wessem, M. v., and Young, D. A.: Deep glacial troughs and stabilizing ridges unveiled beneath the margins of the Antarctic ice sheet, Nature Geoscience, https://doi.org/10.1038/s41561-019-0510-8, 2020.